Astronomical Journal, in press

H I Bright Galaxies in the Southern Zone of Avoidance

P.A. Henning,[1] L. Staveley-Smith,[2] R.D. Ekers,[2] A.J. Green, [3] R.F. Haynes, [2] S. Juraszek,[3] M.J. Kesteven,[2] B. Koribalski,[2] R.C. Kraan-Korteweg,[4] R.M. Price,[1] E.M. Sadler, [3] A. Schröder,[5]

ABSTRACT

A blind survey for H I bright galaxies in the southern Zone of Avoidance, ($212° \leq \ell \leq 36°$, $|b| \leq 5°$), has been made with the 21 cm multibeam receiver on the Parkes 64 m radiotelescope. The survey, sensitive to normal spiral galaxies to a distance of $\sim$ 40 Mpc and more nearby dwarfs, detected 110 galaxies. Of these, 67 have no counterparts cataloged in the NASA/IPAC Extragalactic Database. In general, the uncataloged galaxies lie behind thicker obscuration than do the cataloged objects. All of the newly-discovered galaxies have H I flux integrals more than an order of magnitude lower than the Circinus galaxy. The survey recovers the Puppis cluster and foreground group (Kraan-Korteweg & Huchtmeier 1992), and the Local Void remains empty. The H I mass function derived for the sample is satisfactorily fit by a Schechter function with parameters $\alpha = 1.51 \pm 0.12$, $\Phi^* = 0.006 \pm 0.003$, and $\log M^* = 9.7 \pm 0.10$.

Subject headings: surveys – galaxies: distances and redshifts – galaxies: mass function – galaxies: fundamental parameters – radio lines: galaxies

1. Introduction

The obscuration due to dust and the high stellar density in our Galaxy varies from place to place within the Milky Way. Overall, it blocks our optical view of the extragalactic Universe over $\sim$20% of the sky, somewhat less in the infrared. This "Zone of Avoidance" (ZOA) was recognized even before the nature of the spiral nebulae themselves was understood. This sky

[1]Institute for Astrophysics, University of New Mexico, 800 Yale Blvd, NE, Albuquerque, NM 87131, USA

[2]Australia Telescope National Facility, CSIRO, P.O. Box 76, Epping, NSW 2121, Australia

[3]School of Physics, University of Sydney, NSW 2006, Australia

[4]Departamento de Astronomia, Universidad de Guanajuato, Apartado Postal 144, Guanajuato, Gto 36000, Mexico

[5]Observatoire de la Côte d'Azur, B.P. 4229, 06304 Nice Cedex 04, France

coverage limitation does not pose a problem for the study of galaxies themselves, as there is no reason to believe that the population of obscured galaxies should differ from those in optically unobscured regions. However, to understand the Local Group's motion requires mapping the surrounding mass inhomogeneity, measured in practice by galaxy over- and under-densities, across the entire sky. In particular, the lack of a full census of nearby, hidden galaxies is troublesome, since the local galaxies should play a significant role in the Milky Way's motion with respect to the microwave background (Kraan-Korteweg 1993).

The ZOA has been successfully narrowed by deep searches in the optical and infrared (see Kraan-Korteweg & Woudt 1999 for a comprehensive review of the various efforts). However, optical searches fail where the extinction exceeds 4 - 5 magnitudes, within about $|b| \lesssim 5^\circ$ of the Galactic plane. Near-infrared surveys, e.g. 2MASS (Skrutskie et al. 1997) and DENIS (Epchtein 1997), will eventually produce catalogs of galaxies closer to the plane than is possible with optical searches, but they do not recover the most heavily obscured galaxies, or galaxies of low surface brightness (Schröder, Kraan-Korteweg, & Mamon 1999). Far-infrared surveys become confusion limited by Galactic sources at low latitudes, and the remaining ZOA still covers ~ 10 % of the sky.

Galaxies which contain H I can be found in the regions of thickest obscuration and IR confusion. The technique was pioneered over a decade ago by Kerr & Henning (1987) who showed through a small, pilot survey that completely optically-hidden galaxies could be readily uncovered through the detection of their 21-cm emission. Since then, a spatially complete survey for spirals out to 4000 km s^{-1} has been conducted over the northern ZOA ($30^\circ \leq \ell \leq 220^\circ$, $|b| \leq 5^\circ$; rms noise 40 mJy beam^{-1}) with the 25 m Dwingeloo telescope (Henning et al. 1998, Rivers et al. 1999). The survey uncovered no massive, "Andromeda"-type galaxy in the ZOA, indeed the nearest, previously unknown galaxy revealed by the survey was Dwingeloo 1, a likely member of the IC342/Maffei group (Kraan-Korteweg et al. 1994). The census for nearby, H I-bearing galaxies in the northern ZOA is complete, at least for those galaxies whose redshifts or blueshifts are sufficient to separate their H I signals from Galactic 21-cm emission, at $0 \pm \sim$100 km s^{-1} .

We report here on a somewhat deeper survey (rms noise 15 mJy beam^{-1}) for H I galaxies in the southern ZOA, conducted with the new multibeam receiver on the 64 m Parkes radiotelescope [6] . The angular coverage ($212^\circ \leq \ell \leq 36^\circ$, $|b| \leq 5^\circ$) completes the survey of the great circle of the ZOA for relatively nearby, dynamically important HI galaxies. The present survey discussed here (the "shallow survey") represents the first stage of an ongoing deeper search of the area with the multibeam system. The shallow survey is comprised of the first two scans of a planned 25 scans of the southern ZOA, estimated to be completed in mid-2000. (This full sensitivity survey will be sensitive to spirals to a redshift of $\sim$ 10,000 km s^{-1}). In addition to the astronomical motivation outlined above, the shallow survey serves as a testbed of techniques for the full sensitivity survey.

---

[6]The Parkes telescope is part of the Australia Telescope which is funded by the Commonwealth of Australia for operation as a National Facility managed by CSIRO.

An intermediate-depth survey consisting of four scans of the region $308° \leq \ell \leq 332°$; $|b| \leq 5°$, has been conducted (Juraszek et al. 2000). This region is of particular interest as it contains the predicted position of the core of the Great Attractor (Kolatt, Dekel, & Lahav 1995).

In § 2, the observations and data reduction will be described. The search method and galaxy H I parametrization procedure will be outlined in § 3. The resulting catalog is presented in § 4. Discussion of the galaxy distribution at low Galactic latitudes, the H I mass function derived for the sample, and predictions for the full sensitivity survey are contained in § 5.

2. Observations and Data Reduction

The observations for the survey commenced on 1997 March 22 and were made by scanning the Parkes multibeam receiver in strips of constant Galactic latitude, each of length 8°. The Parkes receiver has 13 independent beams, each with two orthogonal linear polarizations. The receiver rotation was fixed (with respect to the telescope which has an alt-az mount) during each scan such that the rotation angle of the receiver, relative to the scan direction, was 15° at the mid-point of the scan. This meant that the beams rotated on the sky during each scan. Nevertheless, there was sufficient overlap to obtain complete sampling of the entire southern Plane, with approximately uniform sensitivity (see Staveley-Smith 1997). The absence of continuous receiver rotation and axial focussing helped ensure maximum baseline stability. The telescope scan rate was 1 degree/min, so each scan took 8 min to complete. The observations were done in parallel with the H I Parkes All Sky Survey (HIPASS) and a deeper ZOA survey (see http://www.atnf.csiro.au/research/multibeam/ for current information regarding these surveys). Most observations for the shallow survey were completed by 1997 September 4, although some regions were re-scanned as recently as 1999 August 28, because of earlier pointing problems in a few fields.

The footprint of the multibeam receiver on the sky is $\sim 1.7°$, so that each scan maps out an $8° \times \sim 1.7°$ strip of longitude. To obtain full coverage of the southern ZOA, 34 scans were made between Galactic latitudes $-5°$ and $+5°$ at each of 23 separate central longitudes from 216° to 32°. The observing parameters and the area mapped is summarized in Table 1. In total 782 scans, or $\sim$ 104 hrs of data, were obtained for the 1840 deg^2 comprising the survey region. This corresponds to an integration time, when integrated over all 13 beams, of 200 s beam^{-1}, where the beam size, after gridding, has been taken to be $15\farcm5$. (The full-sensitivity southern ZOA survey will comprise 425 scans at each longitude, or approximately 1300 hrs of integration time).

The average system temperature of the multibeam receiver during the observations was $\sim$ 25 K. The average rms noise after Hanning smoothing and away from strong continuum and line sources was 15 mJy beam^{-1}. The velocity range of the observations was -1200 to 12700 km s^{-1}. The channel spacing was 13.2 km s^{-1} and the resolution, after Hanning smoothing, was 27.0 km s^{-1}.

The spectral data were bandpass-corrected, smoothed and Doppler-corrected using AIPS++ LIVEDATA (Barnes 1998). For each beam and polarization, a template bandpass was calculated by taking the median of the surrounding data with $\Delta\ell = \pm 2^\circ$ and $\Delta t = \pm 120$ s. The spectral data were then gridded into 23 cubes, each of size 10° in longitude by 8° in latitude with a pixel size of $4'$. Each output pixel consists of the median of approximately 30 independent (5 s) spectra which lie within a radius of $6'$ of the center of the pixel. The use of the median statistic successfully removes the effect of outlyers, so that interference and bad data were rejected with good efficiency without manual editing of all spectra (which number about 2×10^6 for the shallow survey). For more details, see Barnes et al. (2000).

3. Search Method and Profile Parametrization

The cubes were Hanning smoothed, and each of the 23 smoothed data cubes was searched by eye using the visualization tool KARMA KVIEW (Gooch 1995). (Experiments with automatic galaxy detection algorithms have failed to date in the complicated ZOA, mainly due to baseline instabilities resulting from the presence of strong Galactic continuum sources. The eye/brain system is still far more effective for finding the H I signals). First, Right Ascension – velocity planes were examined, and candidates noted. The selection criterion was a minimum peak flux density of ~ 75 mJy (5σ), with emission extended over two or more channels, or a minimum flux integral of ~ 4 Jy km s^{-1} . The candidates were then checked at the corresponding positions in Right Ascension – declination planes. Candidates which were created by interference or increased noise at the edges of fields were culled. Finally, the one-dimensional profile, flux density versus velocity, was created for each source, and its shape was checked for good sense, since H I galaxies tend to have 2-horned, flat-topped, or Gaussian profiles.

To measure central positions and flux integrals, a zeroth moment map was first made by integrating the cubes in the full velocity range occupied by each galaxy. For most galaxies, which were unresolved, a Gaussian with the same FWHP diameter as the gridded telescope beam ($15\farcm5$) and a DC offset were simultaneously fitted to each zeroth moment map. Five galaxies were found to be significantly extended, and were fitted with Gaussians of arbitrary width. The positional accuracy is $2'$-$3'$, depending on the S/N ratio, and the flux integral uncertainty is $\sim 20\%$.

Using the best-fit position, spectra were then extracted from the cubes using the MIRIAD task MBSPECT (Sault, Teuben, & Wright 1995). For the unresolved galaxies, this spectrum is a weighted average, with the weight dependent on the distance of each pixel from the fitted position. For resolved galaxies, the spectrum is spatially integrated across the galaxy. Velocity widths were then measured at the 20% and 50% levels (W_{20} and W_{50}), relative to the peak signal, using a width-maximizing algorithm (Lewis 1983). In order to correct for the relatively coarse velocity resolution (27 km s^{-1}) of the Hanning-smoothed spectra, downward corrections of 21 km s^{-1} and 14 km s^{-1} were applied to W_{20} and W_{50}, respectively. A central velocity was also measured from the 50% values. All velocities quoted are in the optical (cz) convention.

4. The Catalog

The shallow survey detected 110 galaxies, whose H I parameters are listed in Table 2, and whose profiles are shown in Figure 1. In Table 2, columns contain the following information:

Column 1a: Source name;

Column 1b: Indicates if the galaxy has an optical or IR counterpart within 6 arcmin listed in the NASA/IPAC Extragalactic Database (NED). If the entry is followed by a colon, there is no redshift given in NED for the object, or, for IRAS 13413-6525 (HIZSS 083) and ESO 223-G012 (HIZSS 095), the HI redshift is just outside of the uncertainty indicated in NED;

Columns 2a & 2b: Equatorial coordinates (J2000) of the fitted position;

Columns 3a & 3b: Galactic coordinates;

Column 4: HI flux integral;

Column 5: Heliocentric velocity (cz), the midpoint at 50% of the profile's peak flux density;

Columns 6 & 7: Velocity width at 50% of peak, and at 20% of peak flux density;

Column 8: Distance to the galaxy correcting the velocity to the Local Group frame, and taking H_0 to be 75 km s^{-1} Mpc^{-1};

Column 9: Logarithm of the H I mass;

Column 10: Foreground extinction A_B estimated from the IRAS/DIRBE maps of Schlegel, Finkbeiner, & Davis (1998).

4.1. Completeness and Reliability

Of these 110 galaxies, 29 have optical counterparts listed in NED with matching redshifts. Two more have counterparts in NED with redshifts just outside the quoted accuracy. A further 12 have a cataloged galaxy within 6 arcmin of the HI position, but with no redshift information. The extinction at the positions of each galaxy was estimated from the DIRBE/IRAS maps of Schlegel, Finkbeiner, & Davis (1998). Note that these maps are not calibrated this close to the Galactic plane, so extinction measurements are somewhat uncertain. However, as expected, the extinction is measured to be higher at the positions of the uncataloged galaxies: the median A_B for the cataloged galaxies is 2.9 mag, versus 5.7 at the positions of the uncataloged objects.

An intermediate-depth survey conducted with the multibeam system in a similar way, but with four scans compared to the two discussed here, of the region $308° \leq \ell \leq 332°$; $|b| \leq 5°$, detected 42 galaxies (Juraszek et al. 2000). The intermediate-depth cubes and the shallow survey cubes were searched independently. All 24 of the shallow survey galaxies in this longitude range were recovered by Juraszek et al. , as they should have been, owing to their $\sqrt{2}$ improved

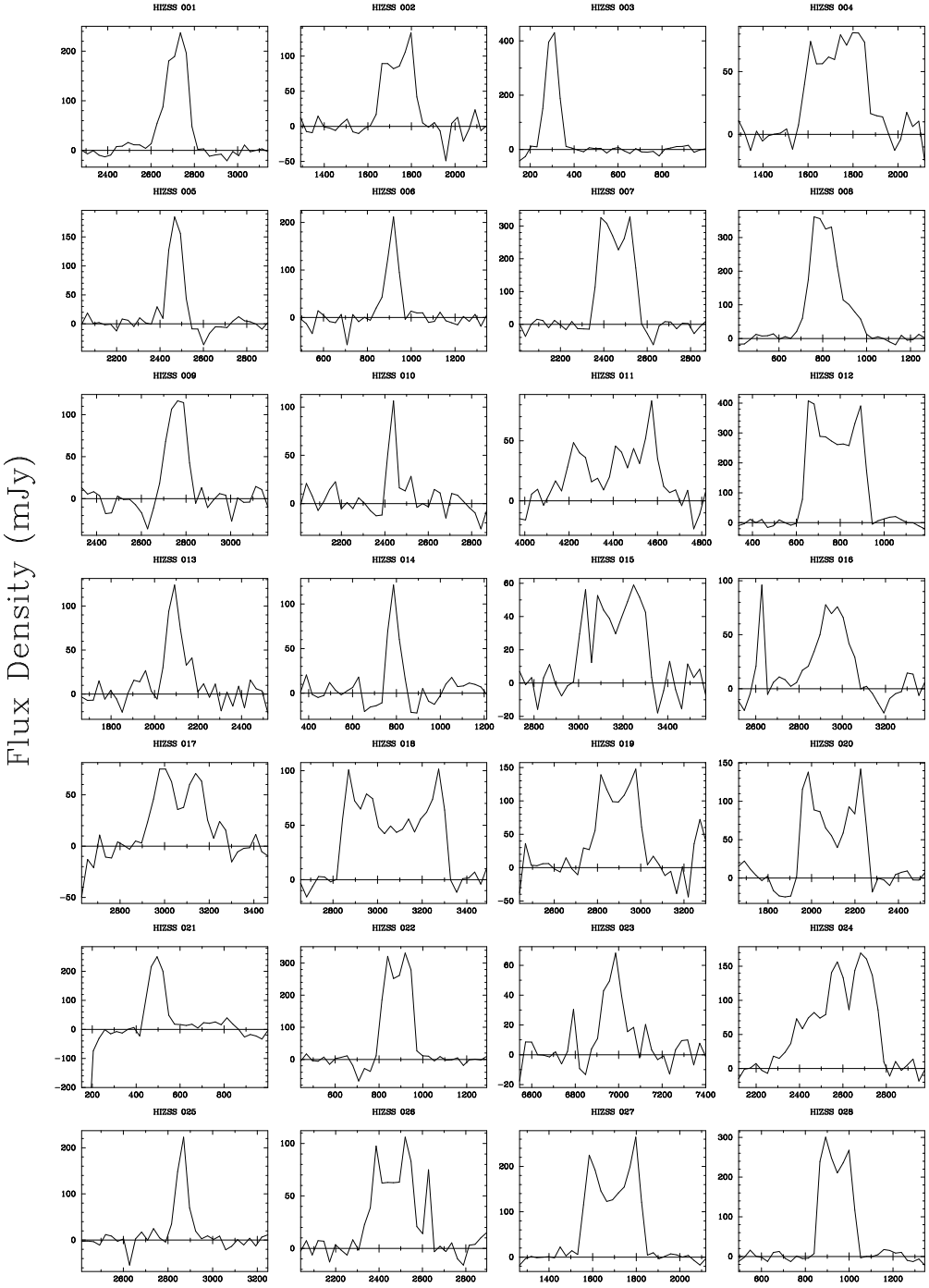
HIZSS 001
HIZSS 002
HIZSS 003
HIZSS 004
HIZSS 005
HIZSS 006
HIZSS 007
HIZSS 008
HIZSS 009
HIZSS 010
HIZSS 011
HIZSS 012
HIZSS 013
HIZSS 014
HIZSS 015
HIZSS 016
HIZSS 017
HIZSS 018
HIZSS 019
HIZSS 020
HIZSS 021
HIZSS 022
HIZSS 023
HIZSS 024
HIZSS 025
HIZSS 026
HIZSS 027
HIZSS 028
Flux Density (mJy)
Velocity (km s^{-1})

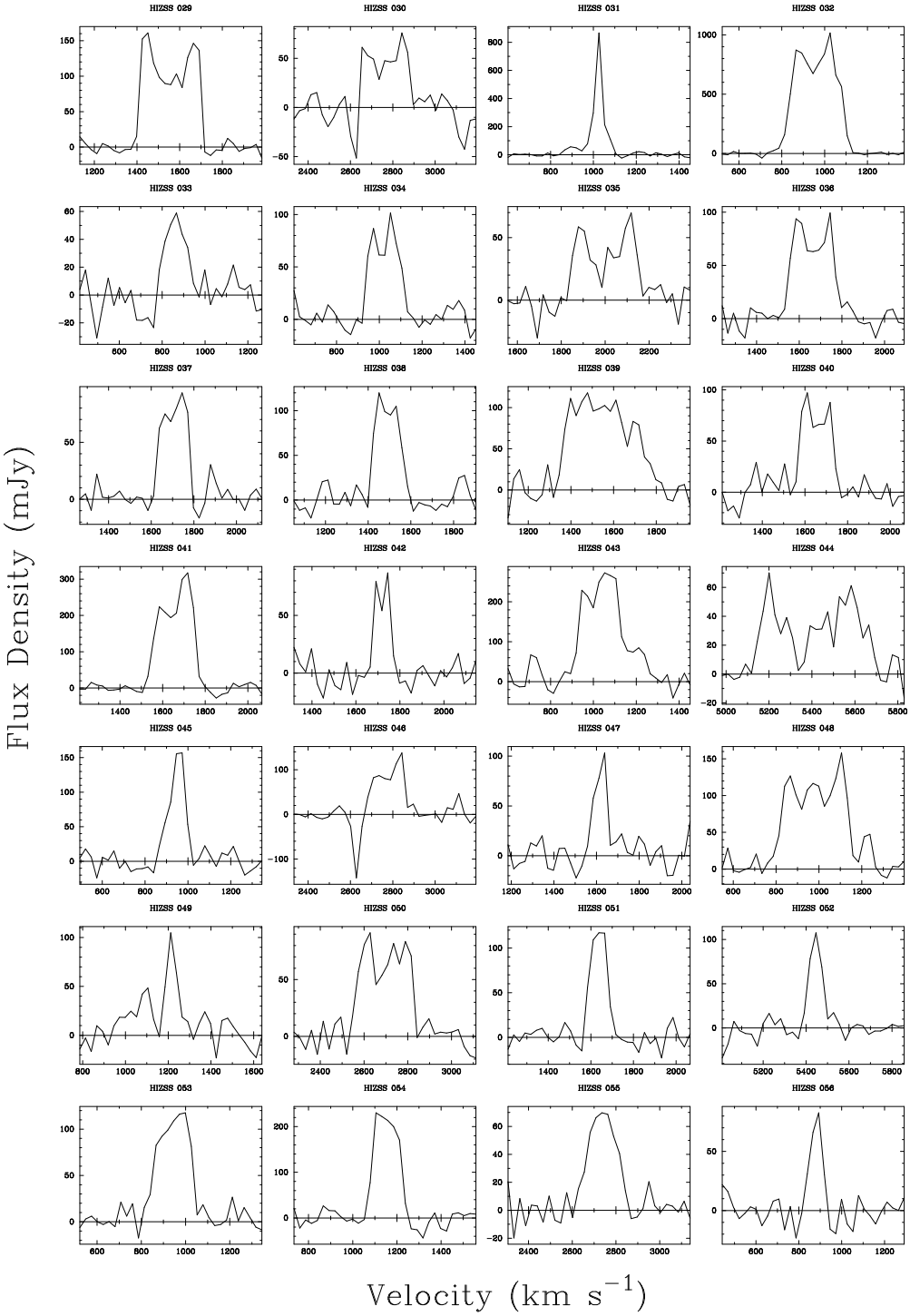
HIZSS 029
HIZSS 030
HIZSS 031
HIZSS 032
HIZSS 033
HIZSS 034
HIZSS 035
HIZSS 036
HIZSS 037
HIZSS 038
HIZSS 039
HIZSS 040
HIZSS 041
HIZSS 042
HIZSS 043
HIZSS 044
HIZSS 045
HIZSS 046
HIZSS 047
HIZSS 048
HIZSS 049
HIZSS 050
HIZSS 051
HIZSS 052
HIZSS 053
HIZSS 054
HIZSS 055
HIZSS 056
Flux Density (mJy)
Velocity (km s^{-1})

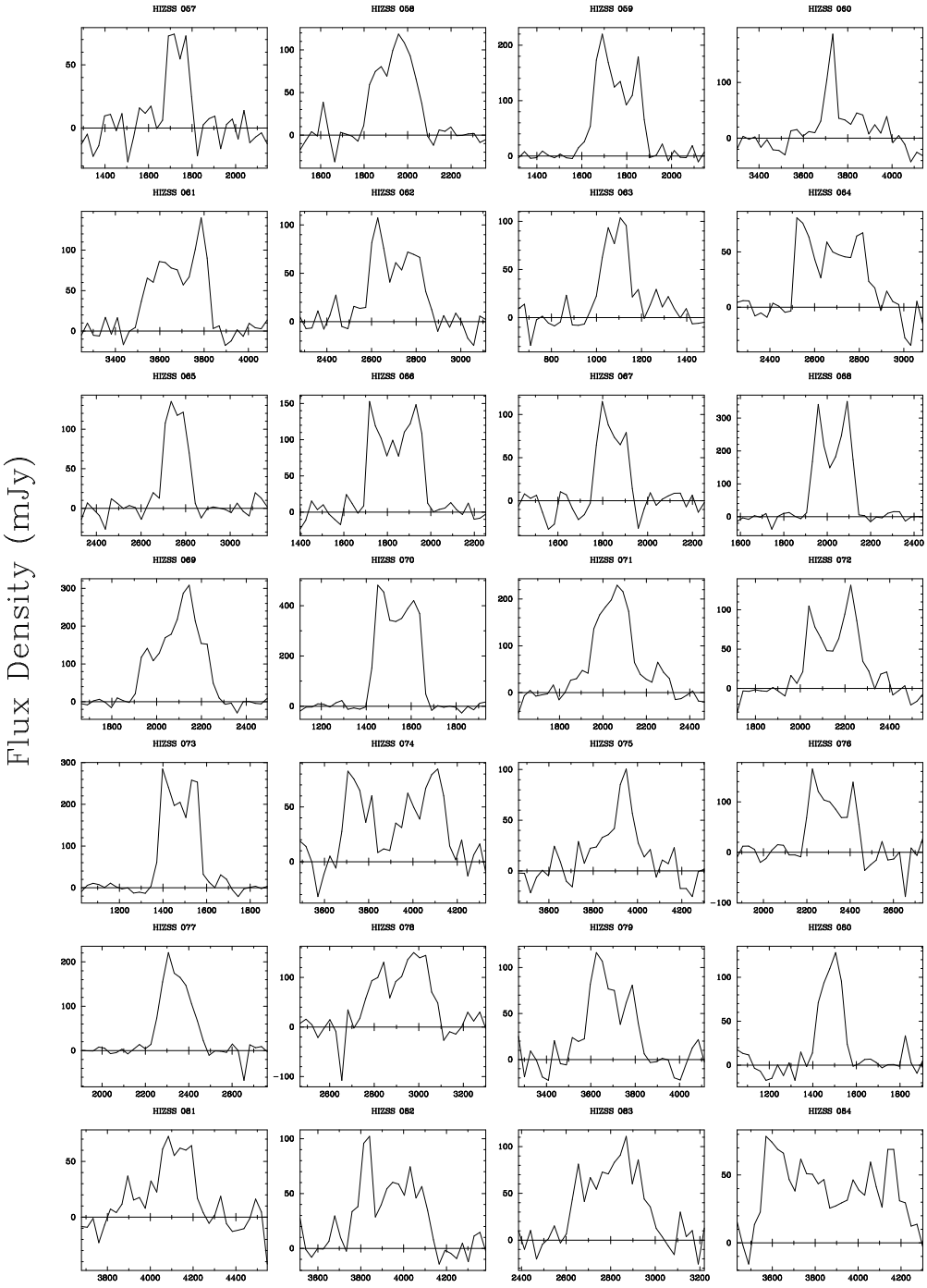
HIZSS 057
HIZSS 058
HIZSS 059
HIZSS 060
HIZSS 061
HIZSS 062
HIZSS 063
HIZSS 064
HIZSS 065
HIZSS 066
HIZSS 067
HIZSS 068
HIZSS 069
HIZSS 070
HIZSS 071
HIZSS 072
HIZSS 073
HIZSS 074
HIZSS 075
HIZSS 076
HIZSS 077
HIZSS 078
HIZSS 079
HIZSS 080
HIZSS 081
HIZSS 082
HIZSS 083
HIZSS 084
Flux Density (mJy)
Velocity (km s^{-1})

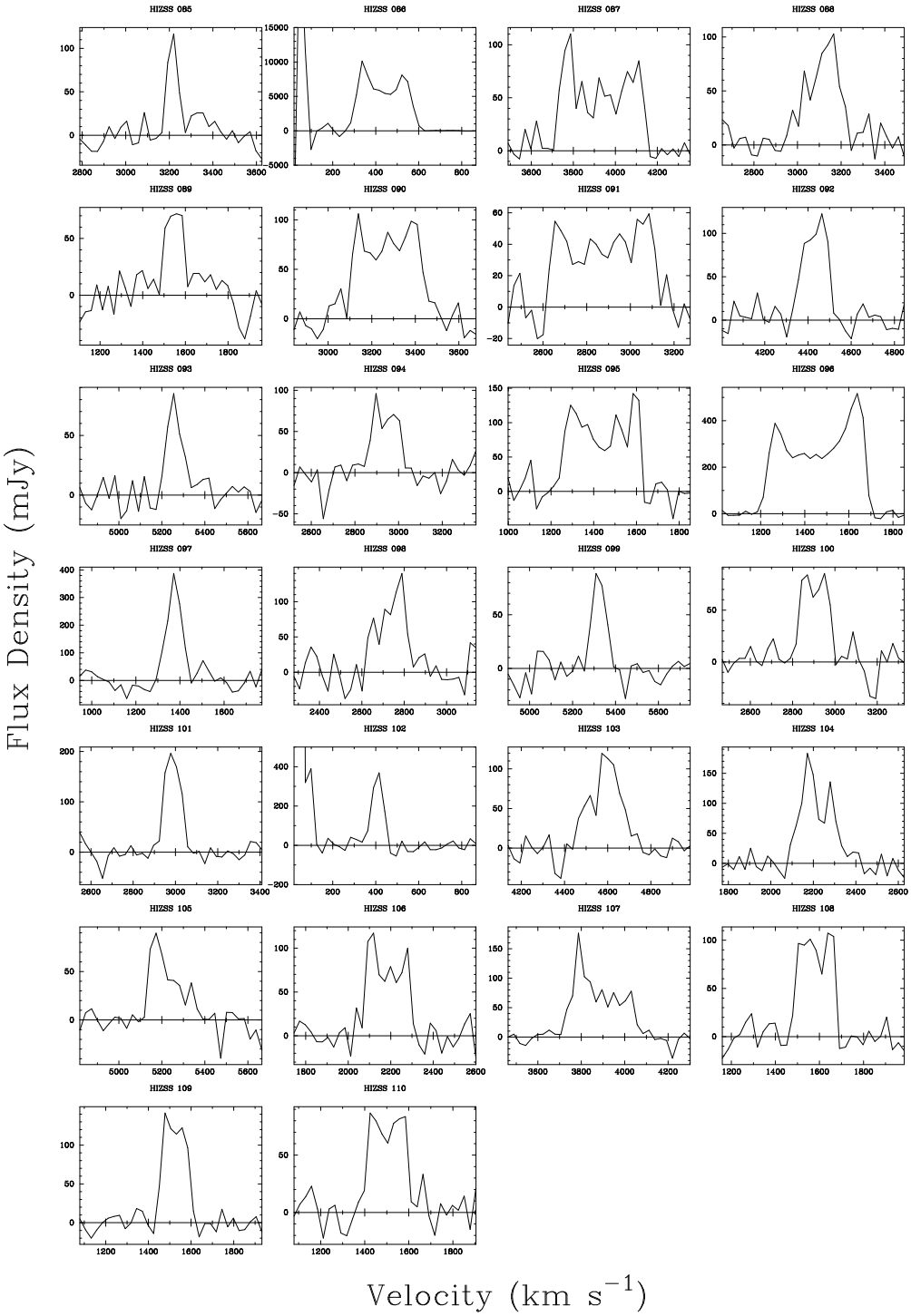

Fig. 1.— H I profiles for the 110 shallow survey detections. Baseline excursions near 0 km s^{-1} and 2650 km s^{-1} for HIZSS 016, 017, 021, 025, 026, 030, 046, 076, 077, 078, 086, 094, and 102 are due to Galactic H I and narrowband interference, respectively.

sensitivity. Of the 18 other galaxies found by this deeper survey, 14 fell well below the selection criteria of the shallow survey. There were four, however, which Juraszek et al. determined to have peak fluxes just at or above the shallow survey flux density cutoff (J1414-62, J1417-55, J1526-51, and J1612-56; cf. Fig 2. in Juraszek et al.). Two of these, J1414-62 and J1612-56, were noted as possible detections in the course of examining the shallow survey cubes, but it was felt they were not quite secure enough for inclusion in the present catalog, the philosophy being that false detections are extremely undesirable. The other two objects were missed. One, J1417-55, while determined to be a broad-profiled galaxy in the intermediate-depth survey, was not recognized as a galaxy by the present work, since only one horn of the profile exceeds 75 mJy, and so appears as a random spike, too narrow for inclusion in this sample. The other, J1526-51, peaks above 100 mJy in the intermediate-depth survey, but has a linewidth of only $W_{50} = 21$ km s^{-1} , and did not satisfy the condition of appearing in at least two channels. Thus the stated selection criteria of the shallow survey are consistent with the results of the intermediate-depth survey in this region.

As a check on the accuracy of the measured parameters, the 21-cm properties of HIZSS 005 (IRAS 07112-0746), HIZSS 008 (IRAS 07232-2422), HIZSS 018 (IRAS 07395-2224), HIZSS 024 (ESO 493-G016), HIZSS 027 (ESO 430-G001), HIZSS 028 (ESO 561-G002), HIZSS 029 (ESO 494-G007), HIZSS 032 (ESO 494-G026), HIZSS 034 (ESO 430-G020), HIZSS 036 (ESO 430-G026), HIZSS 037 (AM 0813-284), HIZSS 038 (ESO 430-G030), HIZSS 039 (NGC 2559), HIZSS 040 (ESO 431-G001), HIZSS 041 (UGCA 137), and HIZSS 044 (ESO 370-G015) were compared with values found in the literature (Garcia et al. 1994, Huchtmeier & Richter 1986, Kraan-Korteweg & Huchtmeier 1992, Staveley-Smith & Davies 1987, 1988, Takata et al. 1994, and Theureau et al. 1998). There is excellent agreement amongst measurements of V_{hel}, W_{20}, and W_{50}, typically within a few km s^{-1} and only rarely differing by more than the velocity resolution. There is more significant scatter amongst H I flux integral measurements, reflecting the measurement uncertainty of the shallow survey ($\sim 20\%$) and in literature values. The HIZSS flux integrals are neither systematically higher nor lower than previously published values.

Table 1. Shallow survey parameters

Parameter	Value
Galactic longitude	$212° < \ell < 36°$
Galactic latitude	$-5° < b < 5°$
Velocity coverage	$-1200 < cz < 12700$ km s^{-1}
Telescope FWHP resolution	14.′3
FWHP resolution in cube	15.′5
Integration time per beam	200 s
RMS noise[a]	15 mJy beam^{-1}
Velocity resolution[a] (FWHP)	27.0 km s^{-1}
Approximate flux density limit	75 mJy beam^{-1}

[a] After Hanning smoothing.

Table 2. Galaxy Parameters from HI Parkes Multibeam Observations

Name Opt/IR	R.A. Dec (J2000)	l b °	Flux Int Jy km s^{-1}	V_{hel}	W_{50} km s^{-1}	W_{20}	Dist Mpc	log M_{HI} $M_\odot$	A_B mag
HIZSS 001 IRAS 06555-0516	06 57 57 −05 20 04	218.42 −0.99	19.2	2720	98	145	33.8	9.7	5.5
HIZSS 002 CGMW 1-0476:	06 59 24 −01 30 15	215.18 1.08	16.7	1736	147	173	20.8	9.2	3.3
HIZSS 003 –	07 00 26 −04 12 17	217.70 0.08	32.1	299	55	85	1.5	7.3	4.7
HIZSS 004 IRAS 07071-0520	07 09 18 −05 25 54	219.80 1.48	20.4	1725	267	297	20.4	9.3	2.0
HIZSS 005 IRAS 07112-0746	07 13 33 −07 51 51	222.45 1.29	12.1	2470	62	83	30.2	9.4	2.7
HIZSS 006 –	07 18 16 −09 04 43	224.07 1.76	12.0	915	41	72	9.4	8.4	1.9
HIZSS 007 NGC 2377	07 24 54 −09 39 51	225.35 2.93	45.7	2457	168	193	29.9	10.0	1.5
HIZSS 008 IRAS 07232-2422	07 25 14 −24 28 25	238.45 −4.01	56.3	805	126	222	7.3	8.9	6.1
HIZSS 009 IRAS 07235-1747: CGMW 1-0879:	07 25 47 −17 53 14	232.70 −0.78	11.3	2756	92	121	33.6	9.5	6.1
HIZSS 010 ZOAG G225.17+03.49:	07 26 38 −09 13 24	225.17 3.51	5.1	2435	27	43	29.6	9.0	1.4
HIZSS 011 CGMW 2-0889:	07 27 39 −23 57 17	238.25 −3.28	14.3	4404	371	423	55.3	10.0	5.3
HIZSS 012 –	07 30 08 −22 00 11	236.80 −1.84	83.7	776	264	284	7.0	9.0	7.9
HIZSS 013 CGMW 2-0978:	07 33 10 −28 39 41	242.99 −4.43	8.6	2089	60	127	24.3	9.1	2.2
HIZSS 014 –	07 36 09 −19 27 23	235.25 0.62	3.4	785	41	68	7.2	7.6	5.7
HIZSS 015 IRAS 07357-1651	07 38 02 −16 57 04	233.29 2.23	14.5	3157	291	313	38.9	9.7	2.8
HIZSS 016 CGMW 2-1059: CGMW 2-1056:	07 38 55 −26 13 12	241.47 −2.13	11.5	2957	146	237	35.9	9.5	3.7
HIZSS 017 IRAS 07377-2435:	07 40 05 −24 41 40	240.27 −1.15	12.3	3062	229	274	37.4	9.6	3.4

Table 2—Continued

Name Opt/IR	R.A. Dec (J2000)	l b °	Flux Int Jy km s^{-1}	V_{hel}	W_{50} km s^{-1}	W_{20}	Dist Mpc	log M_{HI} $M_\odot$	A_B mag
HIZSS 018 IRAS 07395-2224	07 41 47 −22 30 47	238.56 0.26	29.7	3073	451	472	37.6	10.0	2.9
HIZSS 019 –	07 42 34 −34 37 11	249.19 −5.57	24.9	2897	191	233	34.9	9.9	6.1
HIZSS 020 CGMW 2-1147:	07 42 48 −31 57 39	246.89 −4.22	26.0	2099	289	305	24.3	9.6	3.5
HIZSS 021 –	07 46 06 −28 25 35	244.17 −1.84	25.4	491	72	95	2.9	7.7	4.3
HIZSS 022 –	07 46 57 −26 20 01	242.46 −0.63	37.5	884	133	152	8.2	8.8	2.8
HIZSS 023 CGMW 2-1245	07 47 21 −21 37 34	238.44 1.82	7.3	6971	82	148	89.5	10.1	2.6
HIZSS 024 ESO 493-G016	07 48 39 −26 13 41	242.56 −0.25	36.2	2642	225	405	31.7	9.9	2.9
HIZSS 025 –	07 49 38 −35 41 28	250.84 −4.84	11.9	2861	41	70	34.4	9.5	6.3
HIZSS 026 IRAS 07517-2903:	07 53 45 −29 10 03	245.66 −0.78	17.8	2463	180	221	29.2	9.6	3.9
HIZSS 027 ESO 430-G001	07 55 10 −28 09 17	244.96 0.01	48.5	1692	246	276	18.9	9.6	3.7
HIZSS 028 ESO 561-G002	07 55 24 −21 20 25	239.15 3.58	36.6	938	149	171	9.1	8.9	1.5
HIZSS 029 ESO 494-G007	07 56 51 −24 53 15	242.36 2.03	28.9	1556	276	288	17.2	9.3	1.4
HIZSS 030 –	08 01 44 −29 05 05	246.50 0.76	9.3	2764	215	225	33.2	9.4	4.1
HIZSS 031 –	08 05 22 −27 21 13	245.46 2.35	30.4	1024	24	57	10.0	8.9	1.6
HIZSS 032 ESO 494-G026	08 06 12 −27 31 16	245.70 2.42	197.4	961	228	264	9.2	9.6	1.8
HIZSS 033 –	08 07 02 −37 44 47	254.42 −2.93	4.6	862	108	138	7.6	7.8	5.7
HIZSS 034 ESO 430-G020	08 07 09 −28 01 19	246.24 2.33	12.8	1022	147	173	10.0	8.5	2.0

Table 2—Continued

Name Opt/IR	R.A. Dec (J2000)	l b °	Flux Int Jy km s^{-1}	V_{hel}	W_{50} km s^{-1}	W_{20}	Dist Mpc	log M_{HI} $M_\odot$	A_B mag
HIZSS 035	08 09 58	258.05	11.3	1998	281	307	22.7	9.1	5.2
–	−41 41 30	−4.59							
HIZSS 036	08 14 45	249.93	13.4	1660	198	230	18.4	9.0	2.4
ESO 430-G026	−31 20 54	1.89							
HIZSS 037	08 15 55	248.00	9.3	1705	135	150	19.0	8.9	1.7
AM 0813-284	−28 51 25	3.49							
HIZSS 038	08 16 31	247.43	14.7	1488	123	149	16.2	9.0	1.5
ESO 430-G030	−28 05 44	4.02							
HIZSS 039	08 17 12	246.97	28.6	1548	353	414	17.0	9.3	0.9
NGC 2559	−27 26 06	4.51							
HIZSS 040	08 17 41	248.95	11.2	1653	147	165	18.3	8.9	1.4
ESO 431-G001	−29 44 34	3.31							
HIZSS 041	08 17 43	249.26	47.2	1659	174	206	18.4	9.6	1.7
UGCA 137	−30 06 54	3.11							
HIZSS 042	08 20 57	251.92	4.8	1719	68	80	19.1	8.6	1.7
–	−32 51 49	2.13							
HIZSS 043	08 26 28	261.93	41.6	1029	183	314	9.8	9.0	6.5
–	−44 19 23	−3.56							
HIZSS 044	08 28 38	256.35	18.6	5393	448	533	68.0	10.3	3.7
ESO 370-G015	−37 10 30	0.93							
HIZSS 045	08 34 12	257.32	12.7	952	65	114	8.8	8.4	3.8
–	−37 33 48	1.60							
HIZSS 046	08 34 41	259.45	8.4	2779	143	168	33.1	9.3	9.2
–	−40 08 38	0.13							
HIZSS 047	08 55 32	269.47	7.3	1616	57	76	17.6	8.7	7.2
–	−50 01 38	−3.14							
HIZSS 048	08 57 25	261.50	31.8	982	297	332	9.1	8.8	3.2
ESO 314-G002:	−39 16 24	4.09							
HIZSS 049	08 58 04	261.46	6.3	1216	44	72	12.3	8.3	2.7
–	−39 07 29	4.28							
HIZSS 050	08 58 32	266.18	17.3	2696	244	266	32.0	9.6	16.1
–	−45 15 39	0.34							
HIZSS 051	09 01 53	262.72	12.2	1634	83	107	17.8	9.0	2.4
–	−40 08 28	4.17							
HIZSS 052	09 03 30	263.78	7.1	5444	58	80	68.6	9.9	4.5

Table 2—Continued

Name Opt/IR	R.A. Dec (J2000)	l b °	Flux Int Jy km s^{-1}	V_{hel}	W_{50} km s^{-1}	W_{20}	Dist Mpc	log M_{HI} $M_\odot$	A_B mag
–	−41 17 13	3.64							
HIZSS 053	09 17 42	274.26	20.6	944	165	196	8.6	8.6	3.6
–	−53 22 30	−2.85							
HIZSS 054	09 27 58	277.16	27.9	1153	122	146	11.4	8.9	3.9
–	−55 59 26	−3.66							
HIZSS 055	09 37 06	277.19	8.6	2741	145	195	32.6	9.3	8.4
–	−54 37 22	−1.77							
HIZSS 056	09 45 38	273.92	3.1	880	52	78	7.8	7.6	2.0
–	−48 07 27	4.00							
HIZSS 057	09 48 01	278.40	8.1	1734	100	114	19.2	8.8	10.6
–	−54 39 25	−0.77							
HIZSS 058	09 49 12	274.31	20.5	1934	206	248	21.8	9.4	1.5
ESO 213-G002	−48 01 00	4.47							
HIZSS 059	09 49 43	279.79	30.7	1759	203	236	19.5	9.4	9.2
–	−56 32 08	−2.06							
HIZSS 060	09 57 14	275.89	11.7	3725	34	57	45.7	9.8	2.5
–	−48 52 26	4.63							
HIZSS 061	10 04 16	282.57	15.6	3700	225	302	45.4	9.9	15.2
–	−58 33 35	−2.46							
HIZSS 062	10 13 48	280.05	18.8	2707	221	258	32.2	9.7	2.1
ESO 213-G009	−52 18 14	3.42							
HIZSS 063	10 24 59	282.80	10.1	1083	115	175	10.5	8.4	2.7
ESO 168-G002	−54 47 13	2.26							
HIZSS 064	10 37 24	284.40	15.8	2670	310	350	31.7	9.6	3.1
ESO 168-G009:	−54 54 39	3.06							
HIZSS 065	10 39 51	284.52	12.8	2757	105	127	32.9	9.5	2.8
–	−54 31 32	3.57							
HIZSS 066	10 53 42	289.95	32.3	1835	249	263	20.7	9.5	3.6
–	−62 50 30	−2.98							
HIZSS 067	11 30 39	292.61	13.1	1841	131	152	20.9	9.1	3.8
–	−58 46 04	2.48							
HIZSS 068	11 41 14	295.46	41.4	2025	171	199	23.4	9.7	7.9
–	−64 29 02	−2.64							
HIZSS 069	11 49 44	296.23	62.0	2114	157	312	24.6	9.9	10.5
–	−64 00 34	−1.94							

Table 2—Continued

Name Opt/IR	R.A. Dec (J2000)	l b °	Flux Int Jy km s^{-1}	V_{hel}	W_{50} km s^{-1}	W_{20}	Dist Mpc	log M_{HI} $M_\odot$	A_B mag
HIZSS 070	12 02 45	297.19	96.9	1540	202	224	17.0	9.8	11.2
–	−61 40 29	0.65							
HIZSS 071	12 04 16	297.65	32.6	2042	167	211	23.7	9.6	24.8
–	−63 13 10	−0.83							
HIZSS 072	12 13 37	299.03	16.5	2144	223	262	25.1	9.4	3.7
–	−65 33 38	−2.98							
HIZSS 073	12 21 31	299.16	44.4	1476	176	190	16.2	9.4	5.8
–	−59 42 40	2.94							
HIZSS 074	12 45 46	302.29	27.6	3917	449	473	48.9	10.2	24.6
–	−63 05 27	−0.23							
HIZSS 075	13 02 26	304.13	13.7	3941	68	214	49.2	9.9	12.7
–	−64 08 15	−1.29							
HIZSS 076	13 12 49	305.53	16.8	2317	214	238	27.6	9.5	9.8
–	−60 53 42	1.87							
HIZSS 077	13 14 50	305.95	29.1	2337	131	193	27.9	9.7	4.0
WKK 2029	−58 55 47	3.80							
HIZSS 078	13 27 32	307.78	24.4	2915	267	326	35.7	9.9	3.5
ESO 173-G015	−57 31 04	5.01							
HIZSS 079	13 29 56	307.46	18.7	3694	200	235	46.1	10.0	12.5
–	−61 50 46	0.69							
HIZSS 080	13 33 07	308.43	14.3	1482	107	132	16.6	9.0	3.5
–	−58 06 09	4.32							
HIZSS 081	13 37 06	308.88	12.6	4124	155	220	51.9	9.9	3.8
–	−58 31 04	3.83							
HIZSS 082	13 42 14	309.04	14.3	3942	284	355	49.5	9.9	12.0
–	−61 04 58	1.19							
HIZSS 083	13 45 15	308.44	30.2	2789	292	359	34.1	9.9	3.9
IRAS 13413-6525:	−65 39 25	−3.36							
HIZSS 084	13 51 44	310.72	23.8	3869	621	698	48.6	10.1	4.5
–	−58 39 44	3.30							
HIZSS 085	14 07 38	312.70	4.7	3213	44	68	39.9	9.2	8.7
–	−58 43 59	2.69							
HIZSS 086	14 13 27	311.36	1866.6	436	240	278	2.8	9.5	6.1
Circinus	−65 19 09	−3.80							

Table 2—Continued

Name Opt/IR	R.A. Dec (J2000)	l b °	Flux Int Jy km s^{-1}	V_{hel}	W_{50} km s^{-1}	W_{20}	Dist Mpc	log M_{HI} $M_\odot$	A_B mag
HIZSS 087	14 19 42	314.37	16.2	3931	385	413	49.6	10.0	6.6
–	−58 09 58	2.73							
HIZSS 088	14 32 07	316.92	11.4	3109	160	244	38.7	9.6	3.7
ESO 175-G009	−55 29 03	4.63							
HIZSS 089	14 36 12	314.48	7.6	1546	91	103	17.8	8.8	4.6
–	−63 03 58	−2.57							
HIZSS 090	14 52 57	319.03	19.9	3269	311	344	41.0	9.9	6.9
–	−56 46 07	2.26							
HIZSS 091	14 57 07	320.64	23.9	2875	470	489	35.8	9.9	3.7
ESO 176-G006:	−54 24 04	4.09							
HIZSS 092	15 01 27	318.17	14.6	4433	121	153	56.4	10.0	8.4
–	−60 43 22	−1.76							
HIZSS 093	15 04 15	321.04	6.2	5256	62	103	67.6	9.8	6.1
–	−55 27 49	2.67							
HIZSS 094	15 05 54	321.77	8.7	2942	123	151	36.8	9.4	4.2
–	−54 23 34	3.49							
HIZSS 095	15 09 28	323.15	32.5	1440	349	367	16.8	9.3	3.3
ESO 223-G012:	−52 33 27	4.81							
HIZSS 096	15 14 36	323.58	155.4	1457	425	451	17.1	10.0	4.3
IRAS 15109-5248	−53 00 55	4.02							
HIZSS 097	15 32 27	324.10	58.5	1375	58	100	16.0	9.5	78.0
–	−56 01 56	0.08							
HIZSS 098	15 36 51	324.36	14.6	2729	148	189	34.1	9.6	31.2
–	−56 26 19	−0.61							
HIZSS 099	15 40 17	328.08	6.0	5322	62	91	68.9	9.8	3.7
–	−50 51 35	3.58							
HIZSS 100	15 43 10	323.66	9.6	2905	142	158	36.4	9.5	5.0
–	−58 44 24	−2.96							
HIZSS 101	16 05 22	326.47	18.5	2987	83	102	37.6	9.8	2.1
–	−57 51 43	−4.15							
HIZSS 102	16 18 34	329.31	30.3	409	50	71	3.4	7.9	2.7
–	−55 38 44	−3.77							
HIZSS 103	16 20 09	336.01	16.7	4586	147	225	59.5	10.1	9.4
–	−46 21 41	2.67							
HIZSS 104	16 24 33	339.32	21.1	2218	143	210	28.2	9.6	4.8

5. Discussion

5.1. Nearby, H I Bright Galaxies in the Southern ZOA

The shallow survey's rms noise of 15 mJy is equivalent to a 5σ HI mass detection limit of 4×10^6 d^2_{Mpc} $M_\odot$ (for a galaxy with the typical linewidth of 200 km s^{-1}). Thus, the sensitivity to normal spirals falls rapidly beyond about 40 Mpc, and the survey is not well suited to discuss large-scale structure behind the southern Milky Way beyond a few tens of Mpc. The full survey will be sensitive to spirals to a much larger redshift, ~10,000 km s^{-1} , and will be able to address issues such as the Great Attractor, predicted to lie at (l, b, v) ~ (320°, 0°, 4500 km s^{-1}) (Kolatt, Dekel, & Lahav 1995), and other features which may lie hidden (see Kraan-Korteweg & Woudt 1999 for a review of these structures, and Kraan-Korteweg & Juraszek 2000 for preliminary analysis of multibeam full-sensitivity survey detections in the Great Attractor region). However, the shallow survey does now complete the census of nearby, HI bright galaxies which lie at redshifts away from Galactic HI. Sixteen of the 110 galaxies lie at redshifts less than 1000 km s^{-1} and are, therefore, fairly nearby. However, all of the shallow survey galaxies have HI flux integrals an order of magnitude or more below that of the Circinus galaxy, a nearby, massive, low-Galactic latitude galaxy, which is cataloged here as HIZSS 086. One can estimate the dynamical importance of each hidden galaxy without knowledge of its inclination or precise distance by realizing that if the galaxies in the catalog have similar M_{HI} / M_{total}, the gravitational force on the Milky Way due to one of these galaxies is proportional to its HI flux integral. The closest rival in the catalog to Circinus is ESO 494-G026 (Lauberts 1982), listed here as HIZSS 032. It has only about 10% of Circinus's HI flux. (Dynamical analysis of this object to estimate its total mass will be conducted using HI synthesis data obtained with the VLA). All of the newly discovered galaxies have even lower HI flux integrals. No single, previously unknown, dynamically important HI galaxy was found. Five of the 110 galaxies are extended objects at the multibeam resolution, and of these, three were previously cataloged: Circinus, ESO 494-G026, and IRAS 15109-5248. 21-cm follow-up synthesis mapping has been done for IRAS 15109-5248 and the two uncataloged, extended objects, HIZSS 097 and HIZSS 102 by Staveley-Smith et al. (1998). Rotation curve analysis indicates the IRAS galaxy is a massive disk system, estimated $M_{tot} = 6 \times 10^{11}$ $M_\odot$. The other two are moderate to low mass systems, which under the higher resolution scrutiny of the synthesis observations (synthesized beam FWHM ~ 2.2 - 4.5 arcmin) were seen to break up into apparently interacting systems of low H I column density. H I synthesis observations of all of the shallow survey detections using the Australia Telescope Compact Array and the NRAO Very Large Array have been completed or are planned. Identifications on the currently available strips of the southern sky NIR survey DENIS (DEep NIR southern sky Survey; Epchtein 1997) show that many of the shallow survey sources are visible on the NIR images (Schröder, Kraan-Korteweg, & Mamon 1999; Schröder et al. in prep.).

5.2. Large-Scale Structure in the Shallow Survey

Figure 2 shows the distribution on the sky of the shallow survey detections, and galaxies from the literature within a redshift of 4000 km s^{-1} . The shallow survey now fills in the southern ZOA within about 40 Mpc for the first time, with minimal dependence of detection-rate on Galactic latitude (Fig. 3). The Local Void is clearly evident in the distribution of both the optically-cataloged objects, and the shallow survey detections. It is also apparent in Figure 4, the longitude-velocity distribution of the HI detected objects. The three shallow survey objects on the border of the Local Void at l $\sim 30°$ all have redshifts $\sim$ 1500 km s^{-1} , consistent with their being members of the group proposed by Roman et al. (1998). Two of these galaxies lie within the survey boundary of the Dwingeloo Obscured Galaxies Survey, and were also detected by this survey (Rivers, Henning, & Kraan-Korteweg 1999).

The most obvious overdensity of the low latitude galaxies apparent in Figure 2 occurs at l $\sim 245°$. Figure 4 reveals the overdensity is caused by two groupings of galaxies, at (l, v) $\sim$ ($245°$, 800 km s^{-1}) and (l, v) $\sim$ ($245°$, 1500 km s^{-1}). The latter corresponds to the location of the moderately obscured, nearby cluster in Puppis (l, b, v) $\sim$ ($245°$, $0°$, 1500 km s^{-1}) (Kraan-Korteweg & Huchtmeier 1992). This overdensity of galaxies was deduced by Scharf et al. (1992) through a spherical harmonic analysis of IRAS galaxies. The nearer group was also recovered by Kraan-Korteweg & Huchtmeier (1992). There is no evidence of any other nearby, unrecognized clusters of galaxies in the survey region. Except near the Galactic center where continuum emission decreased the sensitivity of the survey somewhat, the survey was uniformly sensitive to spirals with $M_{HI} = 2 \times 10^9$ $M_\odot$ at 1500 km s^{-1} ($H_0 = 75$ km s^{-1} Mpc^{-1}) across the entire southern ZOA, so any hidden overdensities within this redshift range should have been easily detected.

Structures at v $\sim$ 4000 km s^{-1} are not well probed by this survey, however we can see the relative overdensity of galaxies toward the general Great Attractor region, and galaxy underdensity behind the Puppis cluster, broadly consistent with the theoretical mass density reconstructions of Kolatt, Dekel, & Lahav (1995) and Webster, Lahav, & Fisher (1997). The deep survey should definitively confirm or refute the predictions of these and other mass density reconstructions in the ZOA.

5.3. H I Mass Function

To determine the number density of galaxies as a function of H I mass (the H I mass function), the sensitivity of the survey must be carefully determined to be able to apply appropriate volume corrections. Near strong continuum sources, galaxies which would otherwise be detected are hidden in the increased noise. Over the search area, $212° \leq \ell \leq 36°$, $|b| \leq 5°$, 7.7% of the data were disturbed by strong continuum emission, and had rms noise fluctuations a factor of three or more above the quoted sensitivity of 15 mJy. In the volume correction calculations, we take the

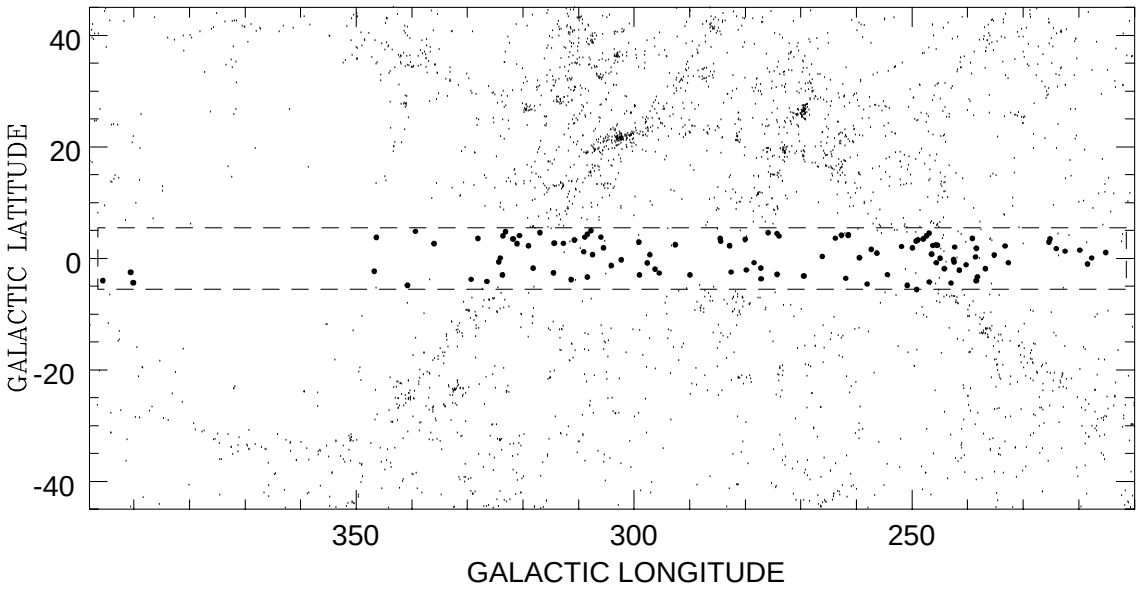

Fig. 2.— Distribution on the sky of cataloged galaxies from the LEDA database within 4000 km s^{-1} (small dots) and shallow survey detections (larger dots). The shallow survey search area is delineated by the dashed rectangle.

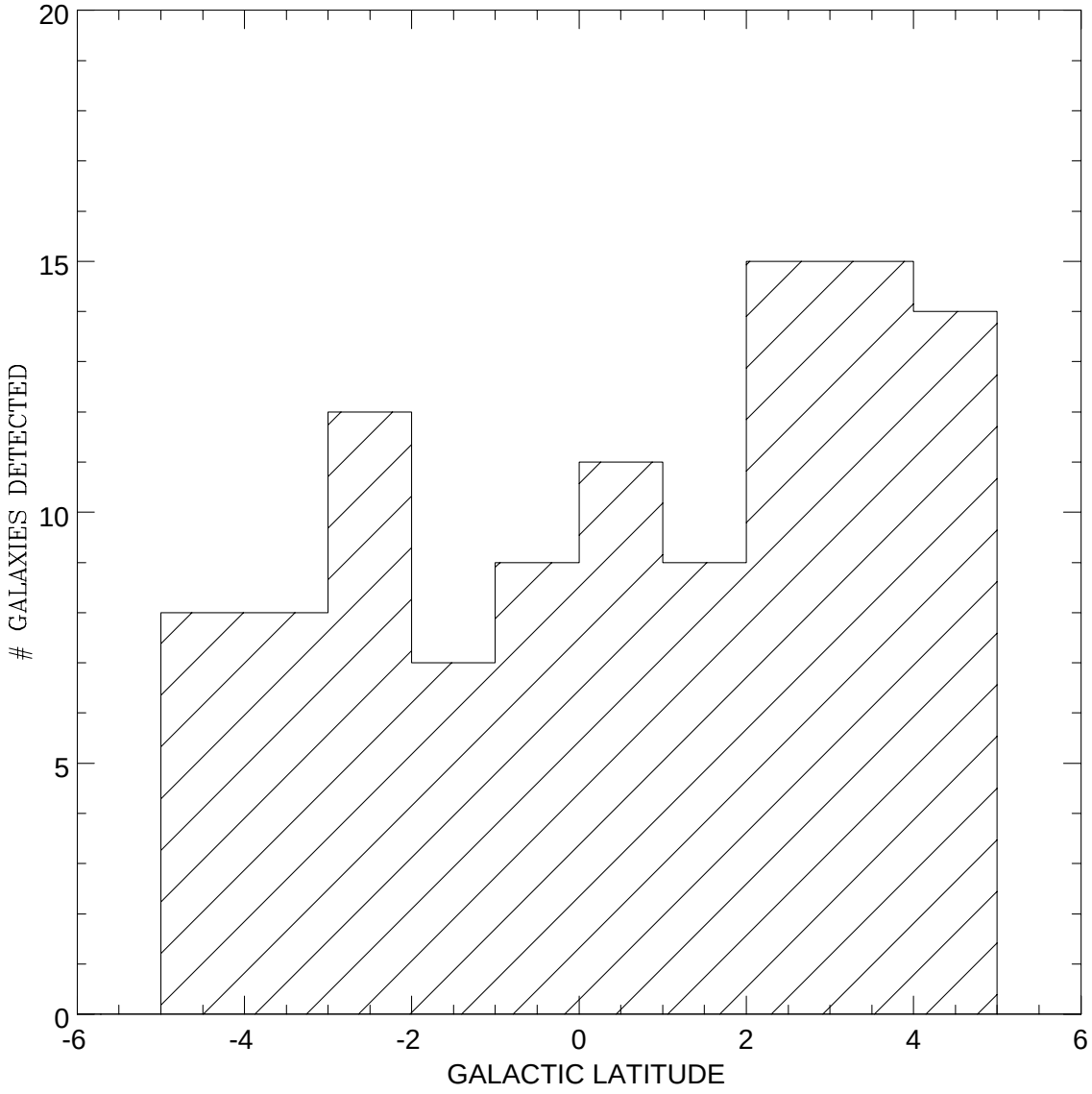

Fig. 3.— Number of shallow survey detections as a function of Galactic latitude.

Table 2—Continued

Name Opt/IR	R.A. Dec (J2000)	l b °	Flux Int Jy km s^{-1}	V_{hel}	W_{50} km s^{-1}	W_{20}	Dist Mpc	log M_{HI} $M_\odot$	A_B mag
–	−42 29 05	4.85							
HIZSS 105	16 53 05	346.34	15.1	5179	75	212	68.1	10.2	6.0
–	−37 57 23	3.79							
HIZSS 106	17 11 46	340.80	16.1	2185	199	213	27.8	9.5	2.9
–	−47 35 24	−4.81							
HIZSS 107	17 19 42	346.77	25.6	3804	66	304	49.8	10.2	11.4
–	−41 17 18	−2.31							
HIZSS 108	18 55 55	30.57	13.7	1582	172	184	23.1	9.2	6.0
–	−03 13 27	−2.47							
HIZSS 109	19 01 48	30.10	13.7	1525	120	142	22.3	9.2	3.5
–	−04 29 51	−4.35							
HIZSS 110	19 10 22	35.55	14.0	1503	177	193	22.4	9.2	2.9
–	+00 30 32	−3.98							

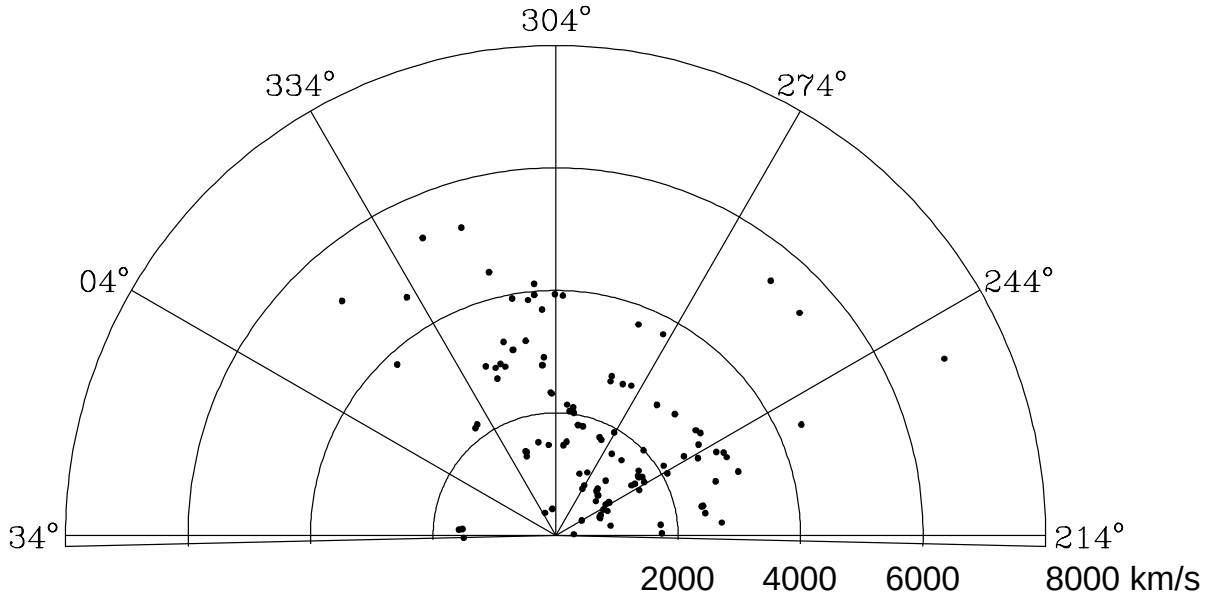

Fig. 4.— Distribution in Galactic longitude and redshift of the 110 shallow survey detections.

survey area to be 92.3% of the area covered by the telescope.

The galaxy selection function for the shallow survey is not based simply on peak flux, but is determined empirically to involve both total flux and linewidth in the following way: $\int$ S dv $\times$ $W_{50}^{-0.7} > 0.3$. Schneider, Spitzak, & Rosenberg (1998) find a very similar functional form for the completeness limit of two previous blind 21-cm surveys done at Arecibo, $\int$ S dv $\times$ $W_{50}^{-0.75}$. With this description, the maximum volume in which each galaxy could be detected is calculated. The average value of V / V_{max} = 0.58, is quite close to the theoretical value of 1/2 for a correctly determined completeness. The resulting number density of H I masses with each galaxy weighted by the inverse of its maximum detectable volume is shown in Figure 5. This H I mass function is well fit by a Schechter function (Schechter 1976) with parameters $\alpha = 1.51 \pm 0.12$, $\Phi^* = 0.006 \pm 0.003$, and log $M^* = 9.7 \pm 0.10$. Note that the Schechter function was not used as an *a priori* assumption of the shape of the H I mass function. The low-mass slope is significantly steeper than the $\alpha = 1.20$ suggested by Zwaan et al. (1997). The densities at the lowest mass bins are consistent with the higher densities found by Schneider, Spitzak, & Rosenberg (1998). The main difficulty remains small number statistics, with the three lowest mass bins of Figure 5 containing a total of six galaxies. With the increased search volume of the HIPASS and full sensitivity ZOA surveys, the statistical robustness of the mass function parametrization will be improved.

5.4. Predictions for the Full Sensitivity Survey

We now estimate how many galaxies should be uncovered by the full sensitivity ZOA survey, to be completed in the year 2000. The deep survey will consist of 435 scans at each longitude, compared with the 34 of the shallow survey. This factor of 12.5 increase in integration time will lead to a $\sqrt{12.5} = 3.5$ improvement in sensitivity. For a galaxy of a given M_{HI} and velocity linewidth, the distance to which it could be detected will increase by a factor of $\sqrt{3.5}$. Thus, the volume increase of the deep survey over the shallow survey is about a factor of 6.5, leading to a rough estimate of $6.5 \times 110 \approx 700$ galaxies to be detected by the deep survey. Indeed, a portion of the deep survey is completed, and the four data cubes in the region of the supposed Great Attractor have been inspected, and about 300 galaxy candidates noted (S. Juraszek, private communication). Extrapolation over the full spatial extent of the survey leads to an estimate of about 1700 galaxies. However, this region of space contains a significant overdensity of galaxies, and much of the final survey volume will contain the Local Void, so the total tally may be closer to 1000 galaxies.

Efforts are underway to develop software tools which model and remove strong continuum sources from the data, which should decrease the effective noise even further, increasing the survey sensitivity and the number of detected objects.

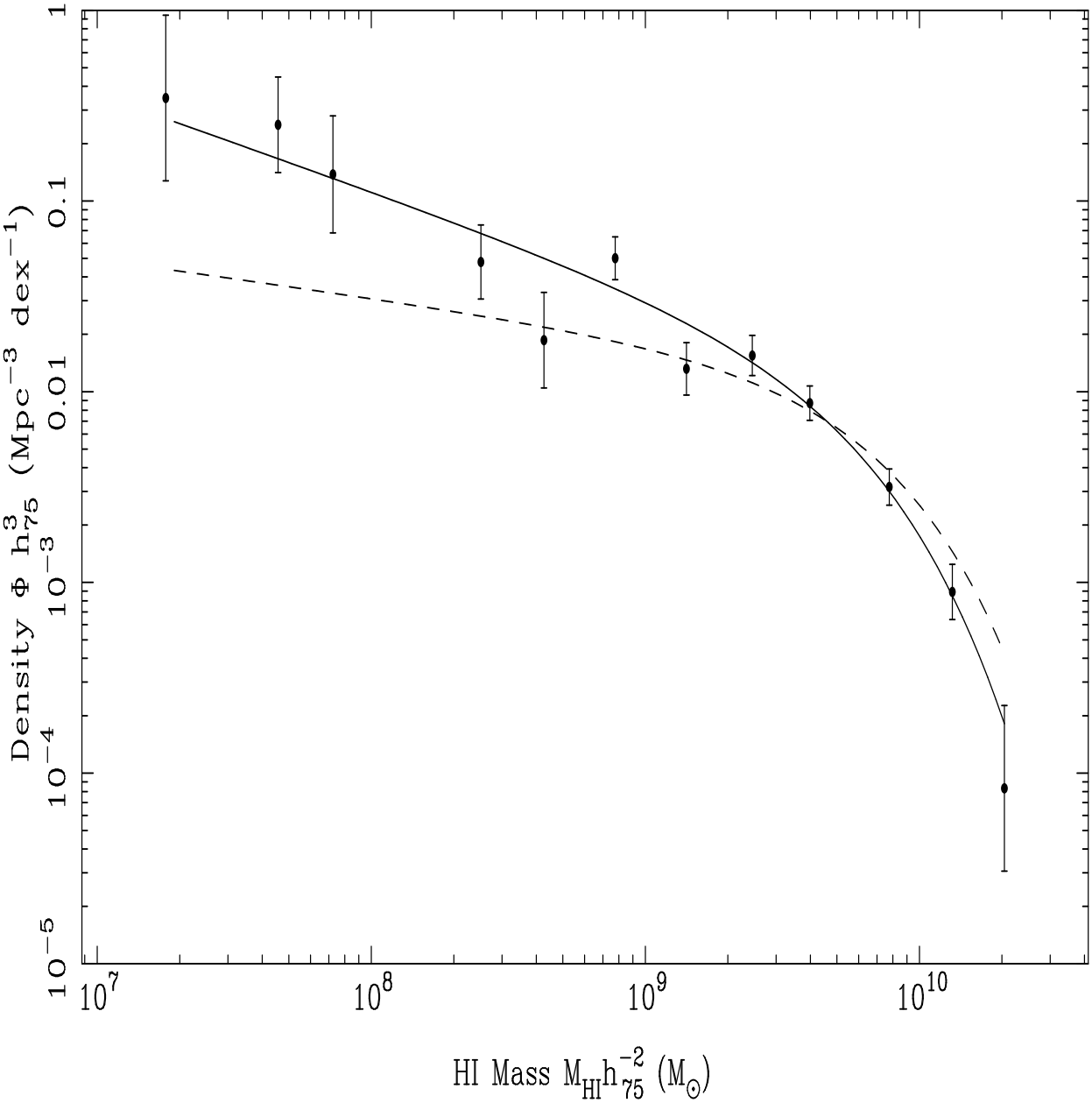

Fig. 5.— H I mass function determined from the shallow survey detections. The errorbars on the points are determined by counting statistics. The function is satisfactorily fit by a Schechter function with $\alpha = 1.51 \pm 0.12$, $\Phi^* = 0.006 \pm 0.003$, and log $M^* = 9.7 \pm 0.10$, shown by the solid curve. The dashed curve shows an H I mass function derived by Zwaan et al. (1997) for a smaller H I -selected sample of galaxies.

Acknowledgements

We thank the HIPASS team (PI: Rachel Webster) for assisting with the observing, and the staff at Parkes for their support. We also acknowledge the AIPS++ group for the development of the basis of the data reduction software and some of the observing software. David Barnes contributed very useful software for the analysis of cube statistics. We are grateful to the multibeam instrument teams, headed by Warwick Wilson, Mal Sinclair, and Trevor Bird.

This research has made use of the NASA/IPAC Extragalactic Database (NED) which is operated by the Jet Propulsion Laboratory, Caltech, under contract with the National Aeronautics and Space Administration. We have also made use of the Lyon-Meudon Extragalactic Database (LEDA), supplied by the LEDA team at the Centre de Recherche Astronomique de Lyon, Observatoire de Lyon. The research of P.H. is supported by NSF Faculty Early Career Development (CAREER) Program award AST 95-02268. P.H. warmly thanks the ATNF for the hospitality and support during her sabbatical stay.

REFERENCES

Barnes, D.G. 1998, in ASP Conf. Ser. 145, Astronomical Data Analysis Software and Systems VII, ed. R. Albrecht, R.N. Hook, & H.A. Bushouse (San Francisco: ASP), 32

Barnes, D.G., Staveley-Smith, L., Ye, T., & Oosterloo, T. 1998, in ASP Conf. Ser. 145, Astronomical Data Analysis Software and Systems VII, ed. R. Albrecht, R.N. Hook, & H.A. Bushouse (San Francisco: ASP), 32

Barnes, D.G., et al. 2000, in preparation

Epchtein, N. 1997, in The Impact of Large Scale Near-Infrared Surveys, ed. F. Garzon et al. (Dordrecht: Kluwer), 15

Garcia, A.M, Bottinelli, L., Garnier, R., Gouguenheim, L., & Paturel, G. 1994, A&AS, 107, 265

Gooch, R.E. 1995, in ASP Conf. Ser. 101, Astronomical Data Analysis Software and Systems V, ed. G.H. Jacoby & J. Barnes (San Francisco: ASP), 80

Henning, P.A., Kraan-Korteweg, R.C., Rivers, A.J., Loan, A.J., Lahav, O., & Burton, W.B. 1998, AJ, 115, 584

Huchtmeier, W.K., & Richter, O.G. 1986, A&AS, 63, 323

Juraszek, S., Staveley-Smith, L., Kraan-Korteweg, R.C., Green, A.J., Ekers, R.D., Haynes, R.F., Henning, P., Kesteven, M.J., Koribalski, B., Price, R.M., Sadler, E.M., & Schröder, A. 2000, AJ, in press

Kerr, F.J., & Henning, P.A. 1987, ApJ, 320, L99

Kolatt, T., Dekel, A., & Lahav, O. 1995, MNRAS, 275, 797

Kraan-Korteweg, R.C., & Huchtmeier, W.K. 1992, A&A, 266, 150

Kraan-Korteweg, R.C. 1993, in The Distribution of Matter in the Universe, ed. G. Mamon & D. Gerbal, (Paris: Observatoire de Paris Press), 202

Kraan-Korteweg, R.C., Loan, A.J., Burton, W.B., Lahav, O., Ferguson, H.C., Henning, P.A., & Lynden-Bell, D. 1994, Nature, 372, 77

Kraan-Korteweg, R.C., & Woudt, P.A. 1999, PASA, 16, 53

Kraan-Korteweg, R.C., & Juraszek, S. 2000, PASA, in press

Lauberts, A. 1982, The ESO/Uppsala Survey of the ESO (B) Atlas, (Garching: ESO)

Lewis, B.M. 1983, AJ, 88, 962

Rivers, A.J., Henning, P.A., & Kraan-Korteweg, R.C. 1999, PASA, 16, 48

Roman, A.T., Takeuchi, T.T., Nakanishi, K., & Saitō, M. 1998, Publ. Astron. Soc. of Japan, 50, 47

Sault, R.J., Teuben, P.J., & Wright, M.C.H. 1995, in ASP Conf. Ser. 77, Astronomical Data Analysis Software and Systems IV, ed. R. Shaw, H.E. Payne, J.J.E. Hayes (San Francisco: ASP), 433

Scharf, C., Hoffman, Y., Lahav, O., & Lynden-Bell, D. 1992, MNRAS, 256, 229

Schechter, P. 1976, ApJ, 203, 297

Schlegel, D.J., Finkbeiner, D.P. & Davis, M. 1998 ApJ, 500, 525

Schneider, S.E., Spitzak, J.G., & Rosenberg, J.L. 1998, ApJ, 507, L9

Schröder, A., Kraan-Korteweg, R.C., & Mamon, G.A. 1999, PASA, 16, 42

Skrutskie, M.F., et al. 1997, in The Impact of Large Scale Near-Infrared Surveys, ed. F. Garzon et al. (Dordrecht: Kluwer), 25

Staveley-Smith, L., & Davies, R.D. 1987, MNRAS, 224, 953

Staveley-Smith, L., & Davies, R.D. 1988, MNRAS, 231, 833

Staveley-Smith, L. 1997, PASA, 14, 111

Staveley-Smith, L., Juraszek, S., Koribalski, B.S., Ekers, R.D., Green, A.J., Haynes, R.F., Henning, P.A., Kesteven, M.J., Kraan-Korteweg, R.C., Price, R.M. & Sadler, E.M. 1998, AJ, 116, 2717

Takata, T., Yamada, T., Saitō, M., Chamaraux, P., & Kazés, I. 1994, A&AS, 104, 529

Theureau, G., Bottinelli, L., Coudreau-Durand, N., Gouguenheim, L., Hallet, N., Loulergue, M., Paturel, G., & Teerikorpi, P. 1998, A&AS, 130, 333

Webster, M., Lahav, O., & Fisher, K. 1997, MNRAS, 287, 425

Zwaan, M.A., Briggs, F.H., Sprayberry, D., & Sorar, E. 1997, ApJ, 490, 173

This preprint was prepared with the AAS LaTeX macros v4.0.